AUTHOR(S):

TITLE:

YEAR:

Publisher citation:

OpenAIR citation:

A prototype telerobotic platform for live transmission line maintenance: Review of design and development

Vikram Banthia[1], Yaser Maddahi[1], Kourosh Zareinia[1], Stephen Liao[2], Tim Olson[1], Wai-Keung Fung[2,3], Subramaniam Balakrishnan[1] and Nariman Sepehri[1]

Abstract

This paper reports technical design of a novel experimental test facility, using haptic-enabled teleoperation of robotic manipulators, for live transmission line maintenance. The goal is to study and develop appropriate techniques in repair overhead power transmission lines by allowing linemen to wirelessly guide a remote manipulator, installed on a crane bucket, to execute dexterous maintenance tasks, such as twisting a tie wire around a cable. Challenges and solutions for developing such a system are outlined. The test facility consists of a PHANToM Desktop haptic device (master site), an industrial hydraulic manipulator (slave site) mounted atop a Stewart platform, and a wireless communication channel connecting the master and slave sites. The teleoperated system is tested under different force feedback schemes, while the base is excited and the communication channel is delayed and/or lossy to emulate realistic network behaviors. The force feedback schemes are: virtual fixture, augmentation force and augmented virtual fixture. Performance of each scheme is evaluated under three measures: task completion time, number of failed trials and displacement of the slave manipulator end-effector. The developed test rig has been shown to be successful in performing haptic-enabled teleoperation for live-line maintenance in a laboratory setting. The authors aim at establishing a benchmark test facility for objective evaluation of ideas and concepts in the teleoperation of live-line maintenance tasks.

Introduction

Safe, reliable and sustainable electricity supply is a prerequisite for continuous economic growth and prosperity of modern societies (Sambo et al., 2012). It is in the common interest to develop outage-free power supplies by efficiently planning maintenance activities. Live-line maintenance is carried out for several reasons, such as changing an insulator, replacement of damaged section of a conductor, testing an insulator, or relocating a conductor to a higher pole. In live-line maintenance, it is imperative that the power transmission system must be always available (Toussaint et al., 2009) under high voltage (69 kV). Inspection and maintenance of an overhead power distribution system, however, is a dangerous task to perform, especially in places with acute climatic conditions preventing human exposure over extended periods of time. Linemen need to utilize appropriate techniques to increase safety and convenience as well as reduce hazards and risks. Therefore, utilities around the world have started to develop and examine the application of robotic systems for the inspection and maintenance of power live distribution networks (Lessard et al., 1995; Takaoka et al., 2001).

The adoption of robotics technology to live power line maintenance is still new and introduces challenges that need investigation. Within the context of robotics technology applied to live transmission line maintenance, Toussaint et al. (2009) presented a number of initiatives to develop robots for transmission line maintenance, including various robotic technologies that have been developed at Hydro-Quebec's research institute (IREQ). Montambault and Pouliot (2003) presented a literature review of innovative devices employed for the performance of live transmission line maintenance.

Over the years, researchers have presented novel designs for live transmission lines inspection and maintenance. Song et al. (2012) developed a mobile robot designed for repairing the overhead transmission lines. This mobile robot was able to travel along the transmission wires, and cross counterweights and splicing sleeves. Jian et al. (2009) presented a novel design of a mobile robot for power transmission lines inspection and maintenance. This robot was designed as a

[1]Department of Mechanical Engineering, University of Manitoba, Canada
[2]Department of Electrical and Computer Engineering, University of Manitoba, Canada
[3]School of Engineering, Robert Gordon University, Aberdeen, UK

Corresponding author:
Nariman Sepehri, Department of Mechanical Engineering, University of Manitoba, Winnipeg, MB R3T5V6, Canada.
Email: Nariman.Sepehri@umanitoba.ca

cable car with two multi-joint arms. Wang et al. (2010) presented an inspection robot called SmartCopter based on an Unmanned Autonomous Helicopter (UAH) for the inspection of transmission lines. Yang et al. (2013) investigated the possibility of using neural network as a self-learning control alternative for the control of inspection and deicing transmission line robot. They proposed a mobile robot based on unique line-walking mechanism for inspecting power transmission lines. The novel mechanism enabled the centroid of the robot to concentrate on the hip joint to minimize the drive torque of the hip joint and kept the robot stable when only one leg is hung on line. Park et al. (2009) presented a new inspection robot system to detect faulty insulators. The developed robotic system adopted a new wheel-leg moving mechanism and a new insulation resistance measurement technique, which made the robot small-sized, lightweight and more superior in insulation and reliability.

In recent times, the research focus has shifted to developing teleoperated systems for live line maintenance owing to its inherent advantages. In general, a teleoperated robotic system consists of: (1) a hand controller at master site, (2) a robot at slave site, (3) a communication channel, and (4) a bilateral control system. At the master side, an operator controls a hand-controller to guide the remote manipulator, and at the slave side, the manipulator emulates the behavior of the master hand-controller. The communication channel connects both master and slave sites, and various types of information (position, velocity and/or interaction force) between the master site and the slave site is exchanged. Therefore, the use of teleoperation wherein the operator is released from direct operation, and only plays the role of supervisor at remote site, is helpful in increasing operator safety, and reducing risks and hazards (Kontz and Book, 2003). In context of telerobotic systems for live line maintenance, Takaoka et al. (2001) designed a dual-arm robotic manipulator installed at the top of a mobile crane for live line maintenance. Aracil et al. (2002) developed a teleoperated system for live-line maintenance, which executes tasks directly on hot lines using a master arm. Lu et al. (2003) developed a live working robot with local automatic and master-slave operation possibilities. The application of teleoperated robotic systems in live power line maintenance has demonstrated to possess advantages such as increasing the operator's safety, and coalescing the accuracy and performance of the system with the intelligence of the operator (Montambault and Pouliot, 2003; Takaoka et al., 2001). The developed teleoperated systems so far have been controlled by direct cables that run through the length of the mobile crane. The concept of wireless communication channel for controlling the slave manipulator has not been adopted in any of the relevant works.

Also, it has been seen in the literature that using hand-controllers capable of generating and applying force to the operator has potential to enhance the performance of telerobotic systems (Kontz et al., 2005). The simplest way to generate the haptic force is to employ the concept of virtual fixtures, which are force signals generated by software to be applied to the operator's hand via the haptic device (Abbott et al., 2007). The virtual fixtures constrain large movements

of the operator's hand into constrained regions or along desired paths defined in the slave manipulator working space (Abbott et al., 2003). The use of virtual fixtures can dramatically raise the level of safety and precision that an operator can achieve (Turro et al., 2001). Virtual fixtures can also be used as a source of guidance and navigation by adding virtual constraints that redirect operator's undesirable movements toward useful directions (Moore et al., 2003). Kang et al. (2004) used virtual fixtures to provide passive constraint to the operator's motion during teleoperation. They found that virtual fixtures could improve accuracy and reduce task completion time for performing decontamination activities. However, such a concept has never been employed for live-line maintenance tasks.

Another subject to be considered when developing a telerobotic system is to how to mount the robotic manipulator to reach the transmission line. The easiest and most prevalent practice is to install the robotic manipulator on top of a mobile crane bucket to perform live transmission line maintenance. The base excitation of the slave manipulator, which would reflect the real motion of the slave manipulator in the field caused owing to effects of wind or elasticity of crane arms in real live-line maintenance, should be taken into account while developing such a system.

After reviewing the relevant literature related to live line maintenance, it has been observed that: none of the literature controlled the remote robot through a wireless communication channel, or employed force feedback to improve performance of the teleoperated system, nor did the base excitation was taken into account. This research has been carried out to incorporate the aforementioned issues in designing a comprehensive teleoperated system for live transmission line maintenance. This paper documents the construction of a state-of-the-art experimental test station for remote live-line maintenance tasks that allows simulation of real maintenance scenarios. The slave system is manipulated by a parallel robotic platform imposing the base position deflections owing to wind and that the delays are imposed on a wireless data transmission. The paper presents primary issues and challenges related to successful design and implementation of such a system, followed by presenting appropriate solutions. The setup allows these solutions to be experimentally validated/verified on a common system; thus, comparison of ideas and approaches is made feasible. The test rig also provides a perfect training platform for linemen to perform teleoperated live-line tasks dexterous in a simulated environment in high fidelity to real working environment. The developed system has the potential to be extended for implementation in other industrial fields such as underwater inspection using ROV (remotely operated vehicles).

The remainder of this paper is organized as follows. In Section 2, common challenges in teleoperation for live-line maintenance tasks are discussed, followed by proposing potential solutions. Sections 3 to 6 detail the features of the test station, and outline the approaches implemented to integrate different components to develop this teleoperated system for various live-line tasks. Detailed assessment of the comprehensive system is discussed in Section 7. Concluding remarks and future work are outlined in Section 8.

Figure 1. A lineman conducting maintenance near energized lines using a hot-stick.

Current practice in live-line maintenance

Traditionally, live-line maintenance tasks are conducted manually by operators working near high voltage power lines (see Figure 1) at a location above the ground. These tasks are performed by using an insulated pole (hot-stick) made of fiberglass. Six typical tasks in live-line maintenance are shown in Figures 2a to 2f. The tasks are: pulling out a cotter pin (Task A), connecting or disconnecting a ball and socket joint (Task B), connecting or disconnecting an insulator (Task C), inserting a cotter pin/hammering (Task D), loosening or tightening a nut (Task E), and twisting a tie wire around an electrical cable (Task F).

Using robotics technology, a hydraulic manipulator can be mounted on top of a live-line truck to perform tasks using a hot-stick, which keeps lineman at a suitable and safe distance from the energized lines. The concept is described in Figure 3. A hot-stick (with associated tools) is attached to the end-effector of a robotic arm. The robotic manipulator is then remotely controlled by a lineman/operator enabling him
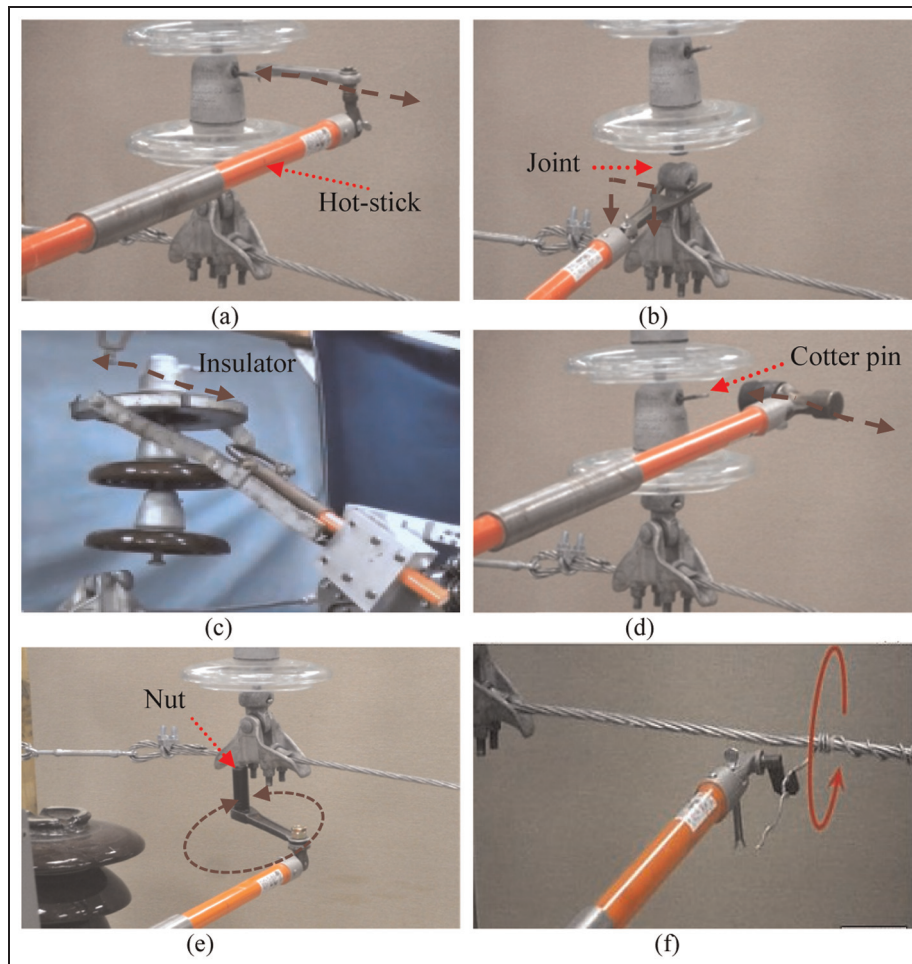
Figure 2. Typical live-line tasks: (a) Task A: pulling out a cotter pin, (b) Task B: connecting or disconnecting a ball and socket joint, (c) Task C: connecting or disconnecting an insulator, (d) Task D: inserting a cotter pin/hammering (e) Task E: loosening or tightening a nut, and (f) Task F: twisting a tie wire around cable.
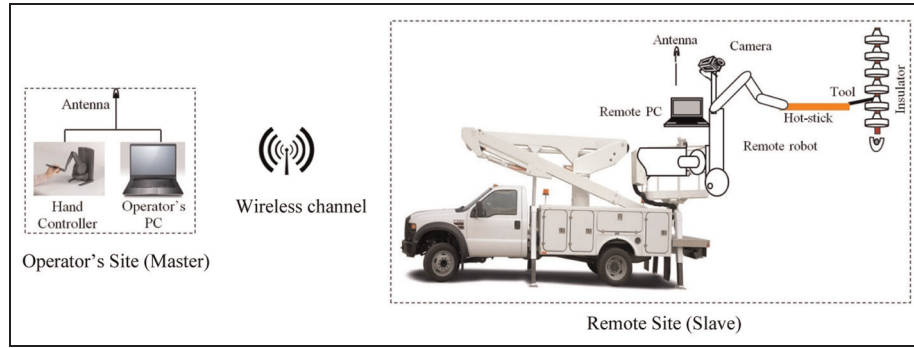
Figure 3. Performing live-line maintenance with teleoperated manipulator. Lineman uses a hand-controller to control manipulator from a distance.
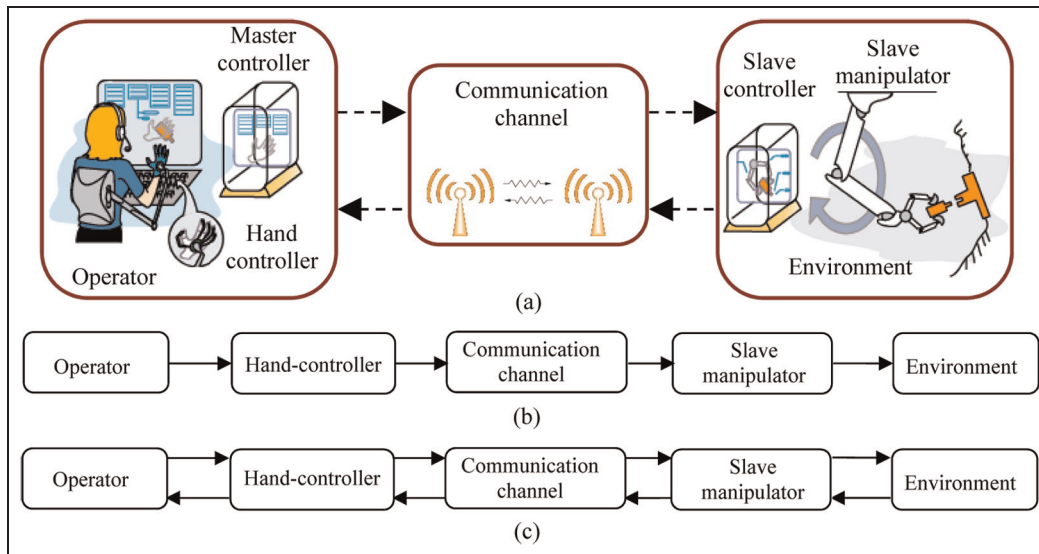
Figure 4. (a) Components of a teleoperated system, (b) unilateral control, (c) bilateral control.

to perform typical live-line maintenance tasks from a safe distance away from the high voltage power lines.

Figure 4a depicts the information flow of the concept shown in Figure 3. As observed, the operator controls the hand controller at the master site, then the communication channel transfers position, velocity and/or force information to the slave site, and the slave manipulator interacts with the environment. Figures 4b and 4c show how information exchanges between master and slave sites in unilateral and bilateral control modes, respectively. In unilateral mode, only information of the master device is sent to the slave side to be used in slave controller, while if the slave manipulator also redirects some information back to the master, by using feedbacks, the system is bilateral (Hokayem and Spong, 2006).

Three main challenges are quantified in developing a general teleoperated system for live-line maintenance. The primary challenge is to design a feedback control system under a situation in which the slave manipulator interacts with the environment or is in free motion. Regarding the position tracking at the slave site, the manipulator may not match the master motion depending on the configuration of the slave manipulator and the malfunction of the control system.

The next challenge is to investigate the effects of communication channel variables on the performance of teleoperated system. Wireless communications inherently have random time delay and packet loss. In a delayed system, there is always a random lag between when an operator perceives the information of slave and when the actual interaction happens. Similarly, the commands sent to the slave are transmitted with a delay too. Moreover, information transmitted between the master and slave sites may be lost because of the random packet loss in wireless channels. Achieving a transparent and stable haptic-enabled teleoperated system owing to delayed and lossy communications channel is a subject that needs be studied for safe and reliable task execution.

Another challenge is the control of the manipulator when placed on top of a crane. In such a configuration, the base will be subjected to unwanted motion owing to wind gust, unstable soil and compliance in the crane actuation. The unwanted motion is highly unpredictable owing to the lack of realistic and accurate models of the working environment. When the manipulator's base is excited, the difficulty in performing tasks naturally increases.
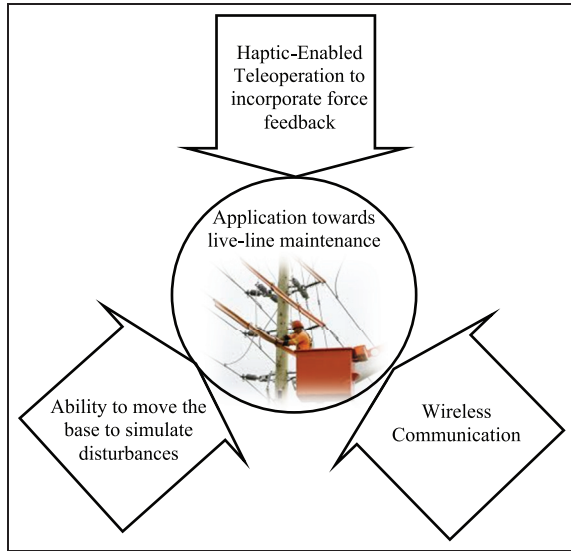
Figure 5. Concept proposed to develop a teleoperated robotic platform to conduct live-line maintenance.

Based on the aforementioned design challenges of teleoperated live-line maintenance robotic system, the following research questions are needed to be addressed (see Figure 5):

(1) How do different types of hand-controllers and mapping systems (joint versus end-effector mapping) affect the performance of a teleoperated manipulator and how to design and employ various force feedback schemes in order to enhance the control of hydraulic telemanipulators?

(2) How to emulate wireless communication channels offering reliable network scenarios and realistic test results, and how to alleviate the effect of wireless communications in teleoperation?

(3) How does the excitation of the slave manipulator base influence the otherwise well-performing teleoperated system?

Construction of the experimental test rig

The first step in developing the proposed comprehensive teleoperated test station is to integrate a hand-controller to remotely control an industrial robot manipulator via a software emulated communication channel.

System overview

Figure 6 shows the telemanipulation system test rig comprising of: ① an industrial hydraulic manipulator (slave site), ② a hand-controller device (master site), ③ a frame replicating a segment of transmission line, ⑤ a hot-stick attached to the robot end-effector, and ⑥ live-line maintenance tools. The tested hand-controllers are a conventional seven-function joystick (see inset in Figure 6) and a PHANToM Desktop haptic device (see ②). The slave hydraulic manipulator shown in Figure 6 is a 6-degree-of-freedom (DOF) Kodiak manipulator. The Kodiak hydraulic manipulator DOFs are: a rotation about vertical axis (arm), three rotations about horizontal axes (shoulder, main elbow, and extended elbow), and two wrist rotations (yaw and roll). In this application, we only used the first 4 degrees of freedom of the manipulator.

On the control front, in order to have the slave manipulator exhibit appropriate dynamic behavior, the controller needs to: (1) have excellent tracking and regulating abilities, (2) respond quickly to variations of the set point, (3) reverse the directions quickly with minimal overshoot, and (4) retain
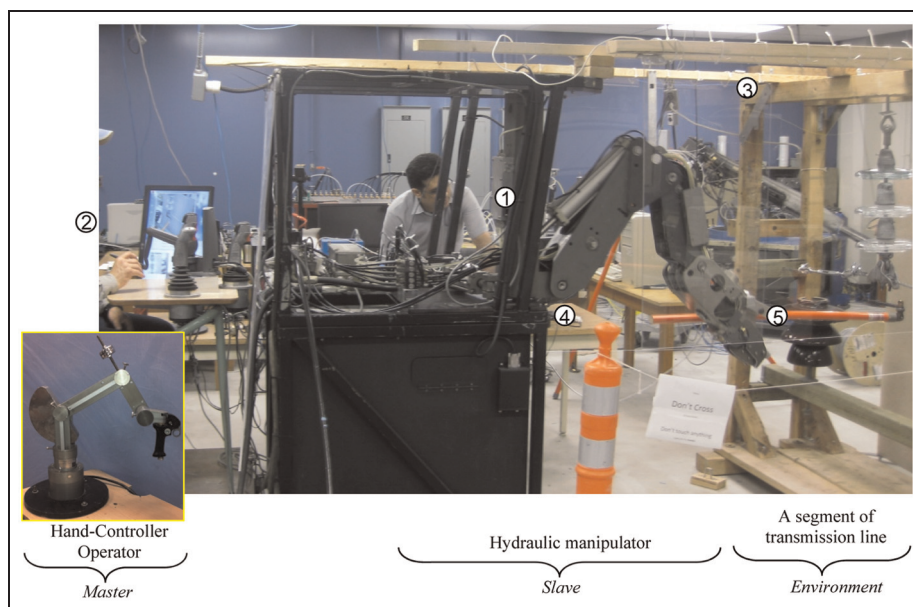
Figure 6. Teleoperated hydraulic manipulator test rig.

the above properties for both large and small changes in set-point. Moreover, in a teleoperated hydraulic system, a human is always in the loop and can control the hydraulic system in any unforeseen or unstructured uncertainties. Thus, the goal while selecting a control scheme for a teleoperated hydraulic application was to arrive at a suitable control algorithm that: (1) requires a minimum knowledge of the machine model, (2) can be easily adopted and tuned in practical situations, and (3) demands minimum computational effort. Conventional PI controllers are widely used in practice owing to their simplicity, reliability and favorable ratio between performance and cost in industrial environments. Three nonlinear modifications to a simple linear PI control law were made, which increased its high-frequency low-amplitude tracking abilities by an order of magnitude. The first modification was to multiply the accumulated error integral by a novel velocity error varying factor at each control step. This modification was shown to effectively prevent integral windup and allows the use of larger integral gains, therefore improving both regulating and tracking abilities. The second modification addresses the problems of hydraulic flow deadband and stiction at the joints. A nonlinear filter was introduced, which reliably detects the occurrence of stalling by calculating a stick-induced velocity error signal. This signal was then used as a switch to boost the control signal as required. Implementing this modification enables the manipulator to follow changes in set-point without any delay. The third modification allows the reduction of overshoot in the deceleration response. This was accomplished by boosting the position error by a factor proportional to a deceleration term in the calculation of the integral portion of the controller at certain periods. The NPI controller was shown to improve tracking accuracy compared with the conventional PI controller. The accuracy of the NPI controller is about 0.2 degrees (Sepehri *et al.*, 1997). The NPI controller was used for each joint of the manipulator.

Several other non-linear controllers have also been developed recently that are applicable for our application and designing and testing such controllers form our future work. For example, to handle unmodeled uncertainties in hydraulics, adaptive robust controllers (ARC) are being widely used today (Cao et al., 2015; Sun et al., 2013; Yu et al., 2013). Yao et al. (2013) designed an integrated direct/indirect adaptive robust controller for both accurate tracking control and excellent parameter estimation, which guaranteed a prescribed output tracking transient performance and final tracking accuracy in both structured and unstructured uncertainties while achieving asymptotic output tracking in the absence of unstructured uncertainties. Also, Yao et al. (2014) proposed a novel feedback nonlinear robust control framework for hydraulic systems with mismatched modeling uncertainties and active disturbance compensation via the backstepping method. The results in this paper provided a new perspective of electro-hydraulic servo control.

There are two configurations designed for experiments:

(1) The master hand-controller and the hydraulic manipulator (slave) are connected to the same PC using parallel port and data acquisition boards, respectively. Therefore, there is no delay or packet loss in

the system. In this case, the control loop works at a frequency of 500 Hz; and

(2) The hand-controller and the slave manipulator are controlled by two different computers. An intermediate computer is also added that receive/ send the data packets from/to master and slave computers. The third computer is used to emulate different scenarios of wireless networks. Network simulator version 2 (NS2) is used to emulate a network scenario.

Effectiveness of the two hand-controllers is evaluated with focus on improving the performance of the overall system when utilized to perform live-line maintenance tasks. The hand-controller is called a "haptic" device if it is capable of producing force. Note that using hand-controllers capable of generating and applying force to the operator (such as the PHANToM haptic device) has shown to potentially enhance the performance of telerobotic systems (Kontz et al., 2005). When information such as position, velocity, force or torque of slave site is transferred onto the haptic device, a sense of telepresence is provided to the operator. Haptic interface has been one of the most effective methods by which the operator can perceive changes in the working environment. Haptic interfaces have been used in wide variety of applications such as hazardous material handling in nuclear services (Clement et al., 1985) medical robotics, tele-ultrasound and tele-surgery (Baheti, 2008; Madhani et al., 1998; Matsumoto et al., 2007; Najafi and Sepehri, 2008; Sun et al., 2007; Tavakoli et al., 2003), underwater robotics (Funda and Paul, 1991), mobile robots (Diolaiti and Melchiorri, 2002; Hong et al., 1999; Lim et al., 2003; Rosch et al., 2002), and micro-manipulation and assembly (Boukhnifer et al., 2004).

Kinematic mapping between master and slave

The teleoperated mapping modes used in this study to examine the different hand controllers are: the joint-mode (JM) and the coordinated-mode (CM). In this work, JM is applied to the conventional joystick and CM is applied to the haptic device. However, both joystick and haptic device can be programmed to operate in either JM or CM mode. In both modes, the NPI position controller is used in controlling the slave hydraulic manipulator.

The joystick has kinematic similarity with the hydraulic manipulator. In JM, the actual angular displacement vector of joystick joint $(\vec{\theta}_a^i)$ is measured by encoders, and sent to the manipulator side as desired angular displacement vector at the slave site $(\vec{\theta}_d^e)$. The error between these two vectors is then used by the position controller to compute control signals for valves of hydraulic actuators for each joint. The slave manipulator end-effector thus travels along the desired path, following the joystick end-effector trajectory in real-time, as shown in Figure 7a.

As illustrated in Figure 7b, the CM uses a PHANToM Desktop haptic device as a hand-controller. Here, the operator moves the haptic device implement. The actual position of the operator's hand is constantly recorded $(\vec{l}_a)$, and then multiplied by mapping factor (α_s) in order to obtain the position of manipulator end-effector $(\vec{E}_d)$. The desired angular
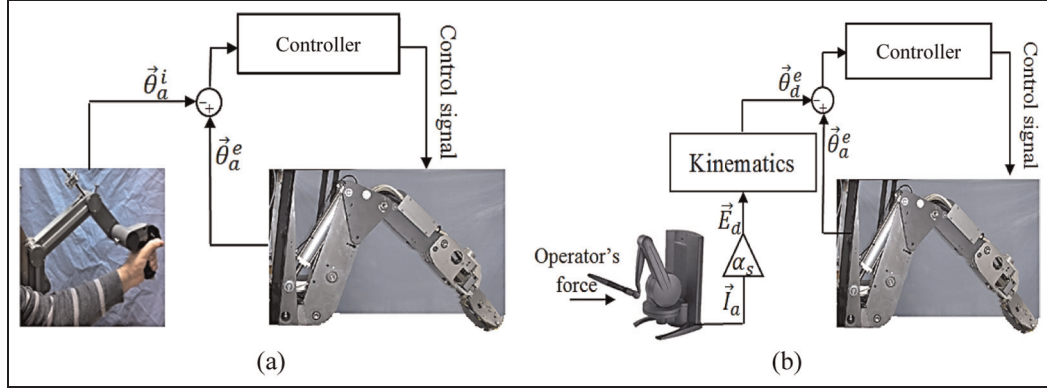
Figure 7. Block diagram of teleoperated hydraulic manipulator using (a) JM and (b) CM.
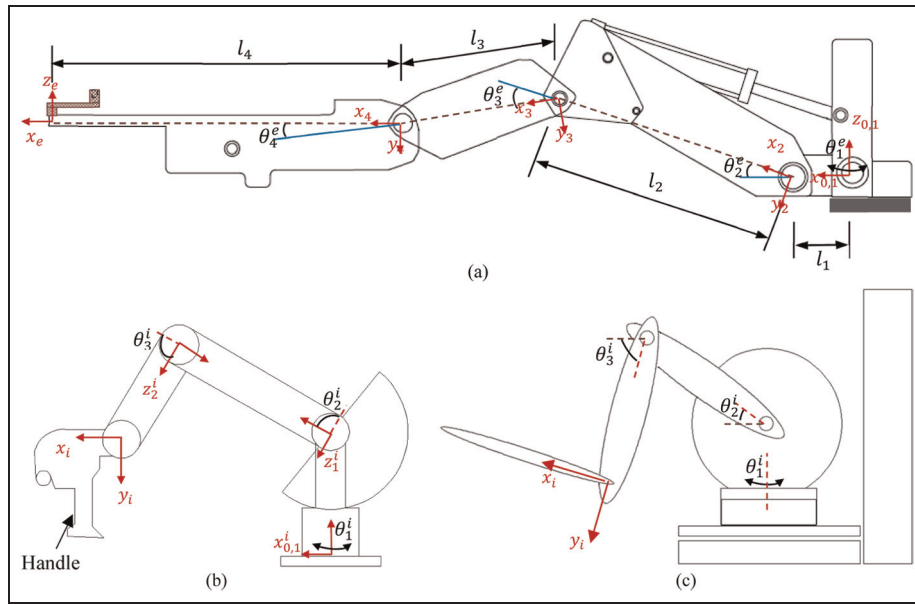
Figure 8. Coordinate frames of (a) slave hydraulic manipulator, (b) conventional seven-function joystick, and (c) PHANToM Desktop haptic device.

displacement vector of manipulator joints $(\vec{\theta}_d^e)$ is then obtained using the inverse kinematics of the slave manipulator shown in Equations (1) to (8) in the next section.

Kinematics

The schematic of slave hydraulic manipulator and the corresponding coordinate frames are shown in Figure 8a. For the conducted experiments, actuators creating the yaw and roll rotations were switched off (a constant desired value was fed to the controller), and only the first four DOFs were employed to run the manipulator. In order to always keep the hot-stick parallel to the horizontal plane similar to the way linemen use it manually, the joint angle θ_4^e (extended elbow) is expressed in terms of θ_2^e and θ_3^e, as follows:

$$\theta_4^e = -\theta_2^e - \theta_3^e \qquad (1)$$

Thus, only the first three angular displacements of manipulator $(\theta_{1,2,3}^e)$ are required to solve the kinematics. In Figure 8a, $\{x_e\ y_e\ z_e\}$ denotes the coordinate system attached to the manipulator end-effector, and the fixed (global) coordinate system is denoted by $\{x_0\ y_0\ z_0\}$. In this section, the superscripts 'e' and 'i' (Figure 8) indicate the parameter belongs to the slave (hydraulic manipulator) and master (hand-controller device), respectively.

Figure 8b depicts the coordinate frames of the conventional joystick. The operator holds the joystick handle and by moving the joystick, values of the first three angular displacements of joystick $(\theta_{1,2,3}^i)$, which are read by encoders, are directly sent as the desired values to the first three joints of hydraulic manipulator $(\theta_{1,2,3}^e)$. Note that (θ_4^e) is calculated using Equation (1). Therefore, when the joystick guides the hydraulic manipulator, all four angular displacements in the slave site can be determined.

Table 1. Specifications of Kodiak 1000 hydraulic manipulator.

Part	Parameter	Value (mm)
Kodiak Manipulator	l_1	133
	l_2	459
	l_3	342
	l_4	1354

Figure 8c depicts coordinate frames of the PHANToM Desktop haptic device. The position of the haptic end-effector $\{x_i \, y_i \, z_i\}$ is mapped onto the end-effector position of manipulator $\{x_e \, y_e \, z_e\}$ by multiplying by a factor, α_s. The actual trajectory of operator's hand at master site (haptic device), thus forms the desired trajectory of manipulator end-effector. Let $\vec{E} = [x_e \, y_e \, z_e]^T$ denote the coordinate of hydraulic manipulator end-effector. The desired angular displacements $\theta^e_{i=1...4}$ are calculated by solving the inverse kinematics of manipulator. Detailed kinematic equations have been reported in (Zareinia et al., 2014). Specifications of Kodiak hydraulic manipulator is shown in Table 1.

$$\theta^e_1 = tan^{-1}\left(\frac{y_e}{x_e}\right) \tag{2}$$

$$\theta^e_2 = tan^{-1}\left(\frac{k_2}{k_1}\right) + tan^{-1}\left(\frac{\pm\sqrt{k_1^2 + k_2^2 - k_3^2}}{k_3}\right) \tag{3}$$

$$\theta^e_3 = tan^{-1}\left(\frac{2l_2k_2c_2 - 2l_2k_1s_2}{k_1^2 + k_2^2 - l_2^2 - l_3^2}\right) \tag{4}$$

Using (1), we have:

$$\theta^e_4 = -tan^{-1}\left(\frac{k_2}{k_1}\right) - tan^{-1}\left(\frac{\pm\sqrt{k_1^2 + k_2^2 - k_3^2}}{k_3}\right)$$
$$- tan^{-1}\left(\frac{2l_2k_2c_2 - 2l_2k_1s_2}{k_1^2 + k_2^2 - l_2^2 - l_3^2}\right) \tag{5}$$

where $c_i = cos(\theta^e_i)$ and $s_i = sin(\theta^e_i)$. In addition,

$$k_1 = x_ec_1 + y_es_1 - l_1 - l_4 \tag{6}$$

$$k_2 = -z_e \tag{7}$$

$$k_3 = \frac{k_1^2 + k_2^2 + l_2^2 - l_3^2}{2l_2} \tag{8}$$

Augmenting the system with force feedback

Three force feedback schemes are employed to enhance the performance of the task. They are virtual fixture (for unilateral teleoperation), augmentation (for bilateral teleoperation) and augmented virtual fixture forces. These schemes have traditionally been employed only in the field of tele-surgery and here, for the first time they have been adopted in live-line maintenance tasks. In the following section, we describe the
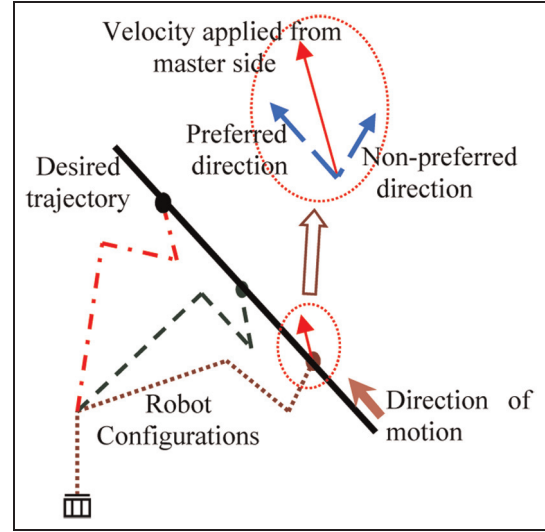
Figure 9. Example of GVF (shown as solid straight line).

concept of these feedback schemes and show their effectiveness.

Virtual fixture

One way to generate the haptic force is to employ the concept of virtual fixture, which constrains large movements of the operator's hand into constrained regions or along desired paths defined in the slave manipulator working space. The concept of virtual fixture was first introduced by (Rosenberg, 1993). In order to understand the concept of virtual fixture, a simple case of a real physical fixture such as a ruler is typically used (Abbott et al., 2003). A simple task like drawing a straight line on a piece of paper without using any tool is generally a difficult task. However, by using a simple device like a ruler, the pen can be guided along a straight line, thus increasing the task accuracy while decreasing the task completion time. Furthermore, without using a ruler, drawing a straight line requires the user to constantly use visual feedback to correct them, and also involves hand-eye coordination. Thus, using a ruler makes the task easier and faster. Moreover, if the ruler is used to guide a cutting tool to cut a work-piece, it works as a barrier to protect against dangerous or destructive failures to increase safety (Li et al., 2007). With respect to live transmission line maintenance application, virtual fixture can be used to define a barrier for the slave manipulator to prevent it from hitting insulators or other elements of transmission lines that can possibly be hazardous or damaging.

In general, virtual fixture is categorized into guidance virtual fixture (GVF), and forbidden region virtual fixture (FRVF) (Abbott et al., 2003; Abbott et al., 2007). In each category, virtual fixture can be further divided into impedance-type virtual fixture, and admittance-type virtual fixture. GVF helps to keep the manipulator on a desired surface or path. As an example of GVF (see Figure 9), the manipulator end-effector must follow a certain trajectory; the
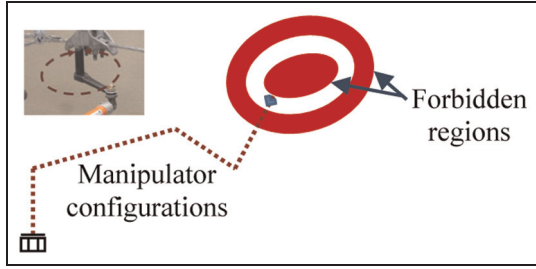
Figure 10. Shaded regions show the FRVR into which the manipulator end-effector should not penetrate.

Figure 11. Virtual spring pulls operator's hand towards desired trajectory. Haptic end-effector position can be on-track ($F = 0$) or off-track ($F \neq 0$). A and B are haptic end-effector actual position (x_a, y_a, z_a) and target (desired) position (x_d, y_d, z_d) respectively.

operator is then able to control the manipulator along the preferred direction while motion along the non-preferred direction is constrained. In admittance-type, the velocity of the manipulator is in direct proportion to the force applied by the operator's hand while in impedance-type, the generated force is proportional to velocity of the operator's hand.

Forbidden region virtual fixture (FRVF) keeps the operator's hand, and thus the slave manipulator, out of a forbidden region of the master/slave workspace. FRVF have no effect on the manipulator when it is out of the forbidden region. In an admittance-type FRVF, the manipulator is not permitted to move into the forbidden region. If the operator forces the master device into the forbidden region, the slave manipulator will not follow the master and halt at the border of the forbidden region. This method is more appropriate where penetration of the slave manipulator into the forbidden region can be particularly damaging, such as tele-surgery. Figure 10 illustrates the admittance type FRVF, where shaded regions are the forbidden regions to which no penetration is permitted.

In an impedance-type FRVF, the force generated is proportional to the manipulator's penetration into the forbidden region. The force can be generated by a virtual spring that pulls the operator's hand back on track or out of the forbidden region. Concept of an impedance-type virtual fixture is described in Figure 11. As seen, the force generated by the haptic device is computed based on the distance between the actual position of master implement, $\overrightarrow{P_A} = \begin{bmatrix} x_a & y_a & z_a \end{bmatrix}^T$, and the desired position of implement, $\overrightarrow{P_B} = \begin{bmatrix} x_d & y_d & z_d \end{bmatrix}^T$. The force can be generated based on the Hooke's law, for instance, as follows:

$$\vec{F} = - G_{VF}\vec{R} \qquad (9)$$

where $F = \begin{bmatrix} F_x & F_y & F_z \end{bmatrix}^T$ represents the force vector applied onto the operator's hand along the reference coordinate system $\{x_R y_R z_R\}$, while G_{VF} is the impedance of the virtual fixture, or basically the stiffness of the virtual spring pushing/pulling the operator's hand toward the desired trajectory. The haptic end-effector position error, $\vec{R}$, is defined as:

$$\vec{R} = \begin{bmatrix} x_a - x_d \\ y_a - y_d \\ z_a - z_d \end{bmatrix} \qquad (10)$$

With reference to Figure 11, when the end-effector is on desired trajectory, the virtual spring remains in rest position
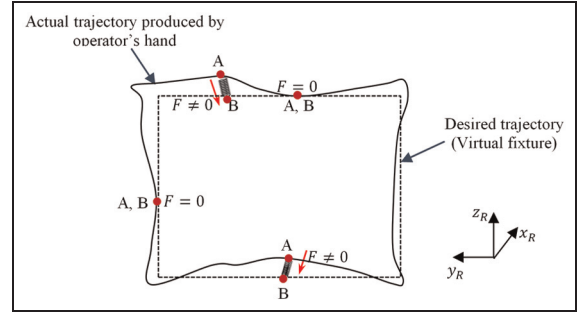
($x_a = x_d$, $y_a = y_d$, $z_a = z_d$), and no force is generated. However, when the operator moves the end-effector away from desired trajectory (off-track), the virtual spring generates a force ($\vec{F}$) that is proportional to the amount of penetration into the forbidden region. In our application, impedance-type forbidden region virtual fixture is used for teleoperation of the hydraulic robot.

Augmentation force

As mentioned earlier, virtual fixture can be used to facilitate certain repetitive task. While the virtual fixture force keeps the operator's hand on the defined virtual path, desired motion at the slave side cannot be assured. For example, the position tracking of the slave manipulator can simply be violated by the fast motion of the operator's hand at the master side reflecting the mismatch between the master and slave dynamics (Maddahi et al., 2016). This is predominantly evident in hydraulic manipulators, since hydraulic actuators exhibit significant nonlinear characteristics (Sepehri et al., 1997). Therefore, to reduce the position errors between the master implement and the slave end-effector, we propose the addition of another force, proportional to the magnitude of the position error at the slave end-effector, however in the direction opposite to the operator's hand velocity vector at the master implement. When position error at the slave end-effector is apparent, the augmentation force is initiated alerting the operator to slow down the hand motion allowing the slave manipulator to catch up. The augmentation force is defined as (Maddahi et al., 2015b):

$$\vec{F}_{AU} = \begin{cases} -\left|G_{AU}(\vec{R}_e - \vec{R}_t)\right|\hat{v} & \|\vec{R}_e\| > \|\vec{R}_t\| \\ 0 & \|\vec{R}_e\| \leq \|\vec{R}_t\| \end{cases} \qquad (11)$$

As shown in Figure 12, $\vec{R}_e$ is the vector of position error at the manipulator end-effector. As the controller has some inherent error, the augmentation force is only generated when the position error is greater than a threshold ($\vec{R}_t$). This threshold is defined based on the steady-state positioning error originating from the manipulator's controller and sensors' resolution and helps to prevent repeated activation-deactivation cycles. When $\|\vec{R}_e\| \leq \|\vec{R}_t\|$, the haptic device does
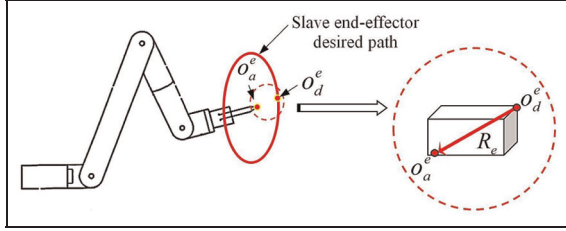
Figure 12. Desired (O_d^e) and actual (O_a^e) positions of the slave manipulator end-effector.
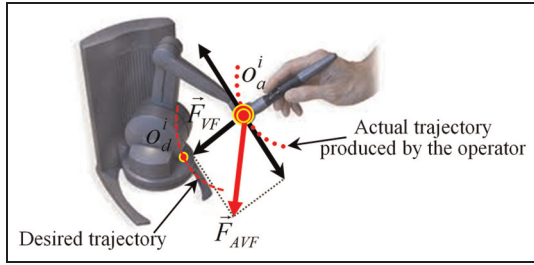
Figure 13. Augmented virtual fixture scheme.

not produce any augmentation force. When $\|\vec{R}_e\| > \|\vec{R}_t\|$, $\vec{F}_{AU}$ is proportional to $\vec{R}_e - \vec{R}_t$ in terms of magnitude, and parallel to $\hat{v}$, which is the unit vector of haptic implement instantaneous velocity. The negative sign specifies that the augmentation force acts in the opposite direction of the haptic device instantaneous velocity. G_{AU} is a diagonal matrix.

Augmented virtual fixture

Indeed, while the virtual fixture is intended to aid the operator in following a predefined path, the proposed augmentation force makes the master dynamics a better match with the dynamics of the hydraulic manipulator. Using this scheme, the combined virtual fixture and augmentation force can reduce position errors at both the master device implement and the slave manipulator end-effector. Figure 13 illustrates how the augmented virtual fixture force is calculated by combining the virtual fixture and the augmentation forces. As shown in Figure 13, the virtual fixture force ($\vec{F}_{VF}$) pulls the operator's hand towards the haptic desired path, while the position referenced augmentation force ($\vec{F}_{AU}$) slows down the operator's hand motion. The augmented virtual fixture force ($\vec{F}_{AVF}$) is then calculated as below:

$$\vec{F}_{AVF} = \alpha_{VF}\vec{F}_{VF} + (1 - \alpha_{VF})\vec{F}_{AU} \qquad (12)$$

where α_{VF} is a positive weighting factor to adjust the relative effect of virtual fixture and augmentation forces.

The overall concept can be summarized as follows: In control of a teleoperated system, actual position of the haptic implement is continuously captured in real-time, while its desired position is obtained by scaling down the slave actual position. This is how the position error at the haptic implement is computed, and used to calculate the virtual fixture

force. On the slave side, the actual position of the slave manipulator end-effector is calculated by substituting the actual angular displacements of joints (see Figure 8) into forward kinematic model of the manipulator. Having the vector of slave position error, the augmentation force is calculated using (11).

Application example I: Testing the developed feedback forces

Two sets of experiments were performed to investigate the effect of adding the virtual fixture force to the system as well as augmenting the virtual fixture with the augmentation force.

Adding virtual fixture. Six experienced linemen from Manitoba Hydro, Winnipeg, Canada, participated in this study. All participants were trained to work with the two hand-controllers, and a brief overview of the concept of virtual fixture, haptics, and operation of the system was provided. The first set of experiments was conducted to examine the performance of the two hand controllers: the seven-function joystick and the haptic device. No force feedback was added to the haptic device. Next, to test the developed feedback force, the operators were asked to repeat the same tasks when virtual fixture (VF) was added to the haptic device while the CM was used to map the master and slave end-effectors.

In JM, the operators were asked to hold the handle of joystick, and move it along the given paths. In force-disabled CM, the participants held the stylus of the haptic device like holding a pen, and follow the given paths while the virtual fixture force was first disabled. The force was then activated, and the participants repeated the same tasks under force-enabled CM. The paths were defined according to real tasks performed by linemen in the field. Figure 14 illustrates typical position errors of manipulator end-effector for the Task F under the three JM, force-disabled CM, and force-enabled CM modes. By comparing the paths depicted in each force mode, it is seen that the operator's hand oscillation, in the JM, is greater than force-disabled CM and force-enabled CM modes. As observed, the position error in the force-enabled CM is smaller than JM and force-disabled CM modes, which in turn are expected to decrease the total operator's effort (Zareinia et al., 2014).

To further quantitatively evaluate the effectiveness of the virtual fixture, other live-line maintenance tasks were conducted. Figure 15 depicts the mean value of each index resulted from experiments. As observed in Figure 15, the task completion time in the JM was more than force-disabled CM and force-enabled CM modes. For instance, in Task A (pulling out a cotter pin), the task completion time for JM, force-disabled CM and force-enabled CM modes were 54.02 sec, 39.89 sec, and 22.61 sec, respectively. Furthermore, the force-enabled CM had less control effort than other modes, and the end-effector travelled the shortest path in the force-enabled CM as compared with JM and force-disabled CM modes. Also, the end-effector average velocity, in the force-enabled CM, was observed to be less than other modes. Therefore,
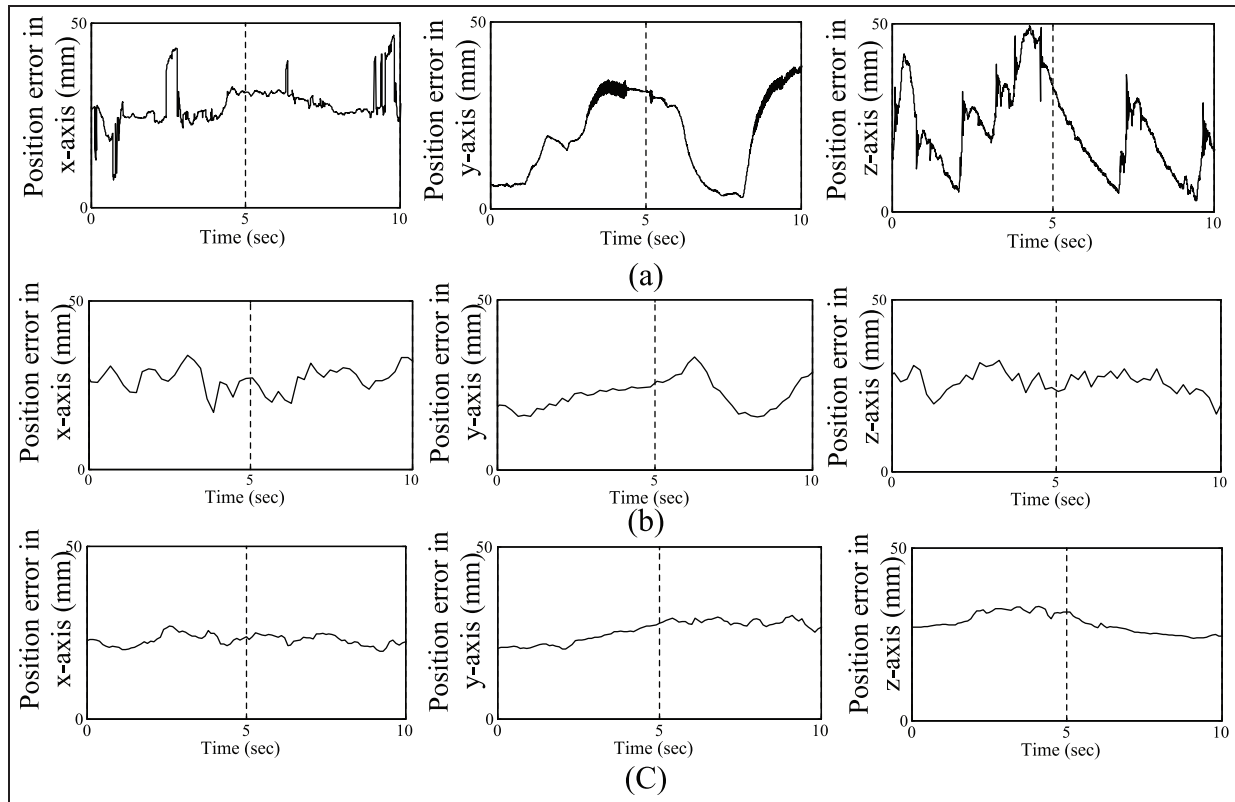
Figure 14. Typical position errors of hydraulic manipulator end-effector under (a) JM, (b) force-disabled CM and (c) force-enabled CM modes in Task F (twisting a tie wire around cable).
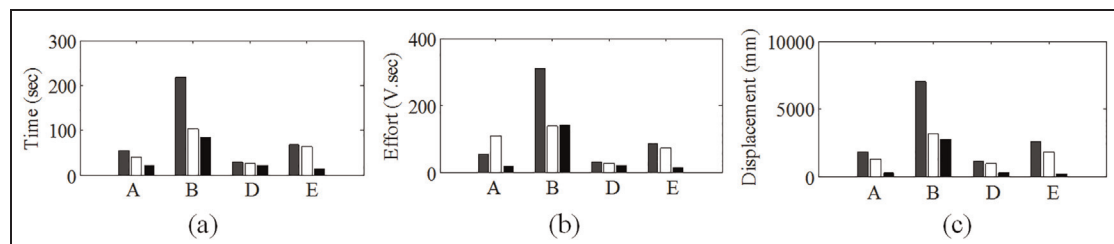
Figure 15. Mean value of each index under JM (left - solid), force-disabled CM (middle - white), and force-enabled CM (right - solid) modes: (a) task completion time; (b) controller effort; (c) total distance travelled by manipulator end-effector.

the manipulator end-effector moved smoother using the force-enabled CM than JM and force-disabled CM modes (Zareinia et al., 2014). In conclusion, the force-enabled CM was found to be the best control mode in terms of defined indices and henceforth the joystick was not used in any of the future tests.

Augmenting virtual fixture with augmentation force. In this set of experiments, the force-enabled CM (virtual fixture force) is augmented by the augmentation force. In total, four typical tasks were performed using the experimental setup, namely Tasks A, B, E and F. Figure 16 illustrates typical position errors of slave manipulator end-effector for the task of loosening and tightening the nut (Task E) under the two force schemes. It is seen that the position error at the slave

end-effector, using the virtual fixture scheme, is larger than the augmented virtual fixture scheme. The augmented virtual fixture scheme reduced position error by guiding the operator to slow down the hand motion allowing the slave manipulator to catch up with the commands coming from the master haptic device (Maddahi et al., 2015b). As expected, as a downside, the task completion time increased when the augmentation force was added to the virtual fixture force (Maddahi et al., 2013b).

Wireless control

As the proposed application of the developed telerobotic system requires working in an outdoor environment, the slave manipulator is aimed to be wirelessly controlled. Wireless
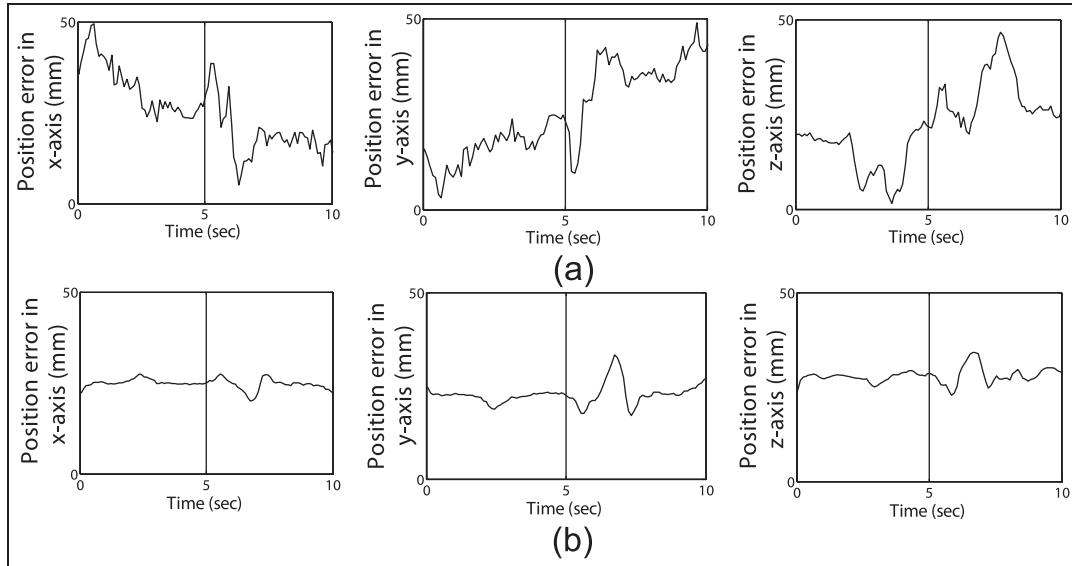
Figure 16. Typical position errors of slave hydraulic manipulator end-effector for Task E under (a) virtual fixture scheme and (b) augmented virtual fixture scheme.

communication is inherently associated with delays and packet losses that vary over time in a random fashion. Delay is the amount of time taken for a data packet to be transmitted from the source to the target, while packet loss happens when data do not reach their intended destination. Both time-varying packet loss and latency, in a wireless network, deteriorate performance of the teleoperated system (Onat et al., 2011; Suzuki and Ohnishi, 2013). Experiments are performed first to evaluate the performance of system based on position tracking of the slave hydraulic manipulator. Then, using experimental results, a lookup table is constructed that allows selecting parameters (like environment obstruction, transmission power of the router, and distance between the master and slave sites) of a wireless network such that a particular value of position error appears at the slave hydraulic manipulator end-effector, which guarantees good transparency (Maddahi et al., 2015a).

Implementation

The network architecture comprises of the master and slave sites connected in a local area network (LAN) using an Ethernet hub, set to send packets to the emulator computer running commercial Network simulator version 2 (NS2) software in the emulation mode (Liao and Fung, 2011). The NS2 mimics the artificial wireless channel and controls when packets are received by the master and slave in order to investigate how delays and losses affect the system response (Breslau et al., 2000).

Emulating wireless channel

The wireless experiments were designed to investigate the effect of changes in parameters of the radio propagation model on the performance of the teleoperated hydraulic

system (Eltahir, 2007). One of the common radio propagation models, shadowing model, was employed. The average received power is assumed to decrease logarithmically with distance. The power received by a receiver antenna (P_r), at a distance of d from a transmitter antenna, is expressed by the Friis free space equation (Rong and Rappaport, 2002),

$$P_r(d) = \frac{P_t G_t G_r \lambda^2}{(4\pi)^2 d^2 L} \tag{13}$$

where P_t and G_t are the transmitter antenna power and gain, respectively. G_r is the receiver antenna gain and λ is the wavelength. L is the system loss factor and d represents the distance between the master and slave sites. This equation is, however, only applicable for short distances and within the far-field of the transmitter antenna (Rong and Rappaport, 2002). But in practice, the surrounding environment clutter may vary even for the same distance between the master and slave sites. Therefore, the power received by receiver antenna is represented as a random and distributed log-normally function (normal in dB), at any distance of d, and defined as follows (Rong and Rappaport, 2002):

$$[P_r(d)]_{dB} = [P_r(d_0)]_{dB} - 10 n log\left(\frac{d}{d_0}\right) + X_\sigma \tag{14}$$

where n is the path loss exponent and d_0 is the reference distance. $P_r(d_0)$ is the received power for a given d_0, and is calculated using Equation (13). X_σ represents a Gaussian random variable with zero mean value, and standard (shadowing) deviation σ (in dB) (Bernhardt, 1987; Cox, et al., 1984). In practice, n and σ are computed from measured data.

In wireless communication systems, a target minimum received power level (P_{min}) is defined, below which, the teleoperated system exhibits instability or poor transparency and
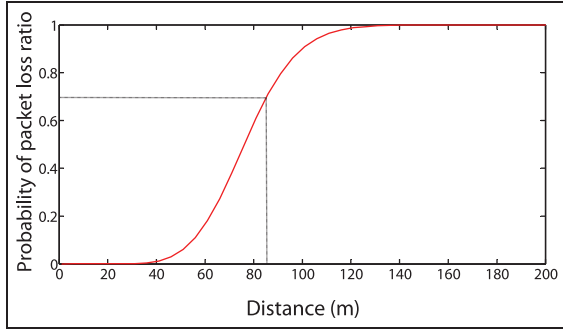
Figure 17. Probability of dropping a packet when $\sigma = 4$, $n = 3.5$ and $P_t = 45$ mW.

Table 2. Lookup table of network parameters.

$n = 2.0$				$n = 4.0$		
P_t mW	d_{35} m	d_{70} m		P_t mW	d_{35} m	d_{70} m
30	417.56	545.62	....	30	44.10	51.46
33	436.08	569.74		33	45.16	52.74
36	453.68	592.72		36	46.24	53.96
39	470.48	614.70		39	47.24	55.14
42	486.58	635.76		42	48.16	56.20
45	502.10	656.04		45	49.06	57.22
48	517.04	675.56		48	49.86	58.24
51	531.50	694.44		51	50.66	59.14
54	545.46	712.68		54	51.46	60.04
57	559.06	730.44		57	52.20	60.90
60	572.24	747.66		60	52.90	61.76

the overall performance is undesirable. The probability that the received signal level will fall below P_{min} is calculated using the equation below:

$$Prob[P_r(d) \le P_{min}]$$
$$= Prob\left[X_\sigma \le 10nlog\left(\frac{d}{d_0}\right) - [P_r(d_0)]_{dB} + [P_{min}]_{dB}\right] \quad (15)$$

Using the above equation, a study was carried out to find the probability of dropping a packet, when P_t was 45 mW and P_{min} and n were set to ã 70 dB and 3.5 dB, respectively, while both G_t and G_r were set to 4. L was equal to 1 and d_0 was set to 1 m. As shown in Figure 17, by increasing the distance, the probability for dropping a packet increases.

Now, for instance, for a known obstruction ($n = 3.5$ dB and $\sigma = 4$ dB) and a given antenna transmission power ($P_t = 45$ mW), the packet loss of 70% is desirable. To find the corresponding distance (d), a horizontal line at packet loss of 70% is drawn that intersects the distribution diagram, as shown in Figure 17. The intersection point gives the distance of 84.9 m, which means that any distance less than 84.9 m is probable to generate a packet loss of less than 70%.

Application example II: Constructing lookup table

Preliminary studies were performed in a field trial to identify the maximum values of time-varying packet loss that do not affect the quality of position signal in teleoperation. It was established that the quality of position signal is satisfactory when the position error at the slave end-effector is less than 30 mm. It is then followed by constructing a lookup table (Table 2) on the basis of identified loss threshold using a graph as in Figure 17. Using this table, for a known pair of n and P_t, the distances at which the network has packet losses of 35% and 70%, can be determined. Table 2 can accordingly be used to select the router type and decide on a proper distance between the master and slave sites, in a known environment. For example, when the slave hydraulic manipulator operates near live lines with n = 2.0 and the operator controls the manipulator at a distance of 450 m, in order to have an acceptable position error, a router with the minimum antenna transmission power of 36 mW should be employed. This is shown in the shaded row in the first column of Table 2.

Studies indicated the system was stable and had good tracking for time-varying packet losses up to 70% (Maddahi et al., 2015a).

Base mobility

Another subject to be considered when developing a telerobotic system is to how to mount the robotic manipulator to reach the transmission line. The easiest and most prevalent practice is to install the robotic manipulator on top of a mobile crane bucket to perform live transmission line maintenance. The base excitation of the slave manipulator, which would reflect the real motion of the slave manipulator in the field caused owing to effects of wind or movements of crane arms, should be taken into account while developing such a system. In the current research, a Stewart platform is used to simulate motion of the crane bucket in live-line maintenance. When the manipulator base moves unknowingly, the difficulty in performing tasks naturally increases. In addition, the base excitation brings about a number of challenging issues when the dimensionality of the hand-controller is added to the teleoperation system.

Stewart platform

Figure 18 illustrates the mobile hydraulic manipulator, a Kodiak manipulator (Figure 18a) that is mounted atop a 6-DOF Stewart platform (Figure 18b). The Stewart Platform is composed of six single-rod hydraulic actuators; each controlled by a proportional valve. Inside each cylinder, a linear displacement sensor is installed that measures the actual position of corresponding actuator. These hydraulic actuators are attached in pairs to three positions on the platform's baseplate, crossing over to three mounting points on a top plate. There are three linear movements (lateral, longitudinal and vertical), and three rotations (pitch, roll and yaw). A computer controls the Stewart platform using a QuaRC interfacing board. The hydraulic manipulator is placed on a corner of the top plate. A schematic of the Stewart platform is shown in Figure 18b. As observed, there are six hydraulic actuators that are commanded to generate the desired posture
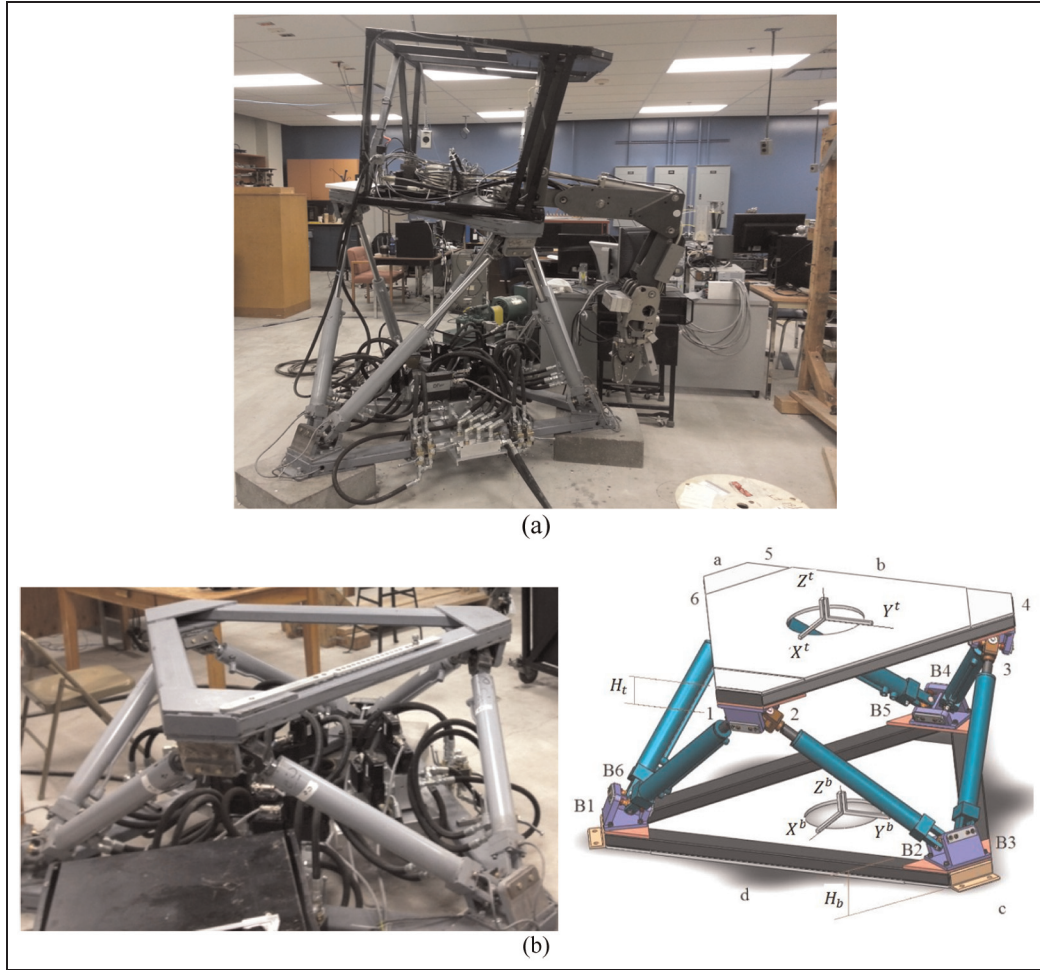
Figure 18. (a) Kodiak hydraulic manipulator mounted atop (b) the Stewart platform.

(position and orientation) of frame $\{X^t Y^t Z^t\}$. The position, D, and orientation, R, of frame $\{X^t Y^t Z^t\}$ with respect to frame $\{X^b Y^b Z^b\}$ are defined as follows:

$$D = (D_x, D_y, D_z) \tag{16}$$

$$R = \begin{bmatrix} \alpha_x & \beta_x & \gamma_x \\ \alpha_y & \beta_y & \gamma_y \\ \alpha_z & \beta_z & \gamma_z \end{bmatrix} \tag{17}$$

With reference to Figure 18b, the length of each actuator, $L_{i=1\ldots6}$, is given by:

$$L_i = |S_i| = \sqrt{S_{i,x}^2 + S_{i,y}^2 + S_{i,z}^2} \tag{18}$$

where,

$$S_i = [S_{i,x} \quad S_{i,y} \quad S_{i,z}]^T = D + T_i R^T - B_i \tag{19}$$

In (19), D and R are given by Equations (16) and (17). B_i and T_i are position vectors of the endpoints of each hydraulic actuator with respect to frames $\{X^b Y^b Z^b\}$ and $\{X^t Y^t Z^t\}$,

Table 3. Specifications of the Stewart platform.

Part	Parameter	Value (mm)
Stewart Platform	Top plate, short side, a	101.6
	Top plate, long side, b	1045.5
	Bottom plate, short side, c	101.6
	Bottom plate, long side, d	1368.0
	H_b	140.5
	H_t	145.8

respectively. They are defined in the Appendix. Specifications of the Stewart platform are given in Table 3.

Application example III: Performance investigation under base excitation

Performances of three control schemes were evaluated in presence of base excitation and delayed network. The schemes were: virtual fixture (VF), augmentation force (AU) and augmented virtual fixture (AVF). The performance of each

scheme was then compared with a scheme in which no force was generated by the haptic device. The effectiveness of each of the three schemes was evaluated by emulating two live power line maintenance tasks in a laboratory setting. The performance of the teleoperated system was evaluated by measuring three indices: task completion time, number of failed trials for each force scheme and displacement of the manipulator end-effector. Two different wireless network scenarios were considered.

Experimental investigations performed on the test rig in the field, indicated that the hydraulic manipulator base was unknowingly excited owing to existence of external disturbances such as wind. The test field indicated that there was a displacement with amplitude of less than 2ã and frequency of about 0.12 Hz (Banthia et al., 2014). Therefore, for designed experiments, the Stewart platform was programmed to generate random displacement (D_x, D_y, D_z). The radial displacement, applied to the top plate of Stewart, has maximum amplitude and frequency of 90 mm and 0.24 Hz, respectively. When the displacement of the top plate is determined, the program solves the inverse kinematics of the Stewart platform and determines the displacement of each hydraulic actuator.

First, the performance was evaluated under no force scheme (NF), whereby haptic device applied no force to the operator's hand. The same tests were repeated when the operator ran the system under VF; that is, a trajectory was defined as virtual fixture, and the operator's hand was kept on the virtual fixture path. The experiments were then repeated when no VF was added to the system, and the haptic device was augmented by the AU. Lastly, the operator was asked to repeat the experiments when the AVF force was utilized by the haptic device.

There were two typical tasks emulated by the experimental setup shown in Figure 19. As shown in Figure 19b, to twist a tie wire around an electrical cable, a semi-circular curve (C-shape path) in $x_0^s z_0^s$ plane is traced. In another task, shown in Figure 19a, the operator pulls the cotter pin out. As seen in Figure 19b, the maintenance tool might collide with the cable because of the manipulator base movement. Therefore, although the virtual fixture part of the scheme intended to keep the operator on the semi-circular trajectory, the operator was forced to move the haptic implement against the virtual fixture force, and deviate from the defined trajectory, in order to avoid colliding. The operators believed that working under virtual fixture and augmented virtual fixture schemes was tiring because of applying such a resistive force over a long time.

Experiments showed that the NF scheme was less time consuming than the other force schemes. In contrary, AVF scheme showed longer task completion times as compared to the AU and VF schemes. The reason can be found in the nature of AVF that: (1) helps the operators to slow down the hand motion when position error appears at the slave site, and (2) tries to pull back the operator's hand toward the virtual fixture trajectory, and therefore diverts the hand from its intended motion.

In terms of distance travelled by the slave end-effector, in both tasks, end-effector travelled longer in NF scheme than the other schemes, while in the AVF scheme it travelled the least. The displacements of the end-effector, for VF and AU
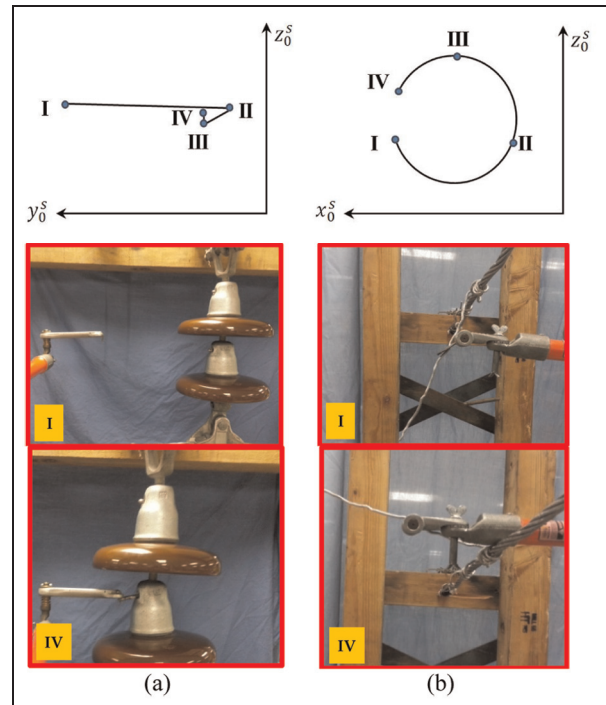
Figure 19. (a) Pulling out a cotter pin (Task A); (b) Twisting a tie wire (Task F).

schemes, were almost close to each other. The number of failed trials, in VF, was more than the other schemes. More specifically, the operators failed the operation, under the VF, AVF, NF and AU schemes, for 22, 17, 13 and 5 times, respectively. With reference to results obtained from the three performance measures, especially the number of failed trials, the AU scheme was found better than the other schemes. Thus, once the base excitation is added to the teleoperated manipulator, augmentation force scheme works the best.

Performance assessment of the system in changing a 3-bell string insulator

The complete system setup includes an operator positioned to view the wireless monitors (see Figure 20). The operator ① has direct visual access to the robotic arm and hot-stick tool as well. The haptic device ② was used to interface with the robotic arm to direct the tool. In addition, the augmentation force was added to the haptic device to reduce the position error at the manipulator's end-effector. Multiple wireless cameras may be positioned on the robot to provide the operator with the best visual feedback ③. In this work, only one camera was used for demonstration purposes. The computer monitor displays the pre-programmed virtual work zone set up to limit the robot movement to a prescribed region. Finally, the hydraulic manipulator ⑤ completes the setup and performs the tasks, translating the operator's hand movements to the hot-stick tool. There are two hot-sticks attached to the arm to receive various hot-stick tools: the pan tool ⑥ for transferring and manipulating insulator strings, and the
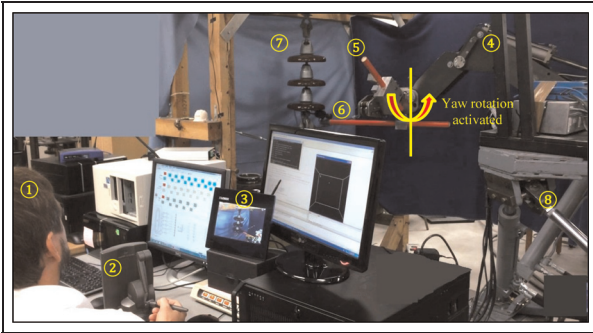
Figure 20. Complete system setup; ① operator ② haptic device ③ cameras ④ manipulator ⑤ pan tool attachment ⑥ multi-tool ⑦ insulator ⑧ Stewart platform.
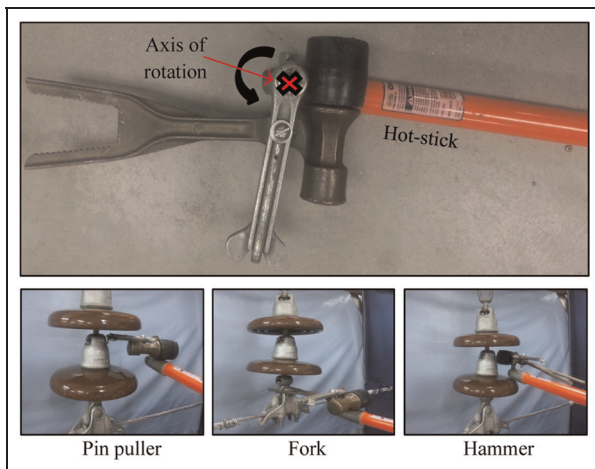
Figure 21. Developed multi-tool is used to perform multiple live-line maintenance tasks.

multi-tool ⑥ for cotter pin and other hardware manipulation. The tasks were performed on a 3-bell string ⑦ in this laboratory demonstration.

Special tools were combined to provide a single multi-tool (see Figure 21) capable of performing several tasks without interrupting or reconfiguring the setup. The cotter pin puller was combined with the hammer head for removal and installation of the cotter pin keeper on the insulator. Lastly, the ball socket adjuster (fork) allows the operator to manipulate the socket for release or capture of the ball on the insulator.

The actuator creating the yaw rotation was switched on this time and the pan tool was attached on that link, so that all the operations required for changing the insulator could be performed without reconfiguring the setup. The pan tool (Figure 22) was used to remove the insulator or insulator string from the Y-ball or adjacent insulator as required. It was then used to transfer and install the new insulator string. As mentioned, the Stewart platform ⑧ simulates the crane bucket movement. Corresponding work envelope and end-effector trajectories are also shown for each task, which demonstrates that with minimal movements, all the tasks were effortlessly performed. The operator began by unpinning the insulator keeper using the multi-tool pin puller, Task A (Figure 23). Inset shows how the operator's hand movement corresponds to the hydraulic manipulator. End-effector motion and corresponding work envelope is shown in Figure 24.

Next, the lower end of the string was released (Figure 25) from the conductor shoe using the ball socket adjuster (fork) (Task B). The haptic device allows the operator to make small positional changes to the hot-stick tool in any direction as though the hot-stick were a pen in hand. Complete three-dimensional motion and control was provided by the hydraulic robotic arm. Normally, the operator's whole body would be involved in manipulating the hot-stick tool from the bucket, ladder or tower. Using the new system, the operator's wrist was most active. This greatly reduced worker's fatigue.

Once the lower end of the insulator string was disconnected, the pan tool was attached and maneuvered into place (Task C), as shown in Figure 26. The string was picked off of the Y-ball connector. Upon removal of the defective string, the pan tool was re-charged with a new insulator (Task C) and the operator now maneuvers the socket, capturing the Y-ball connector (Figure 27).

Finally, after changing the tool attachment from the pan tool back to the multi-tool, the lower attachment is made using the ball socket adjuster (fork) (Task B). Once the socket is seated, the hammer completes the task, driving home the cotter pin keeper (Task D), as shown in Figure 28. This successfully completes the task of the changing an insulator string.
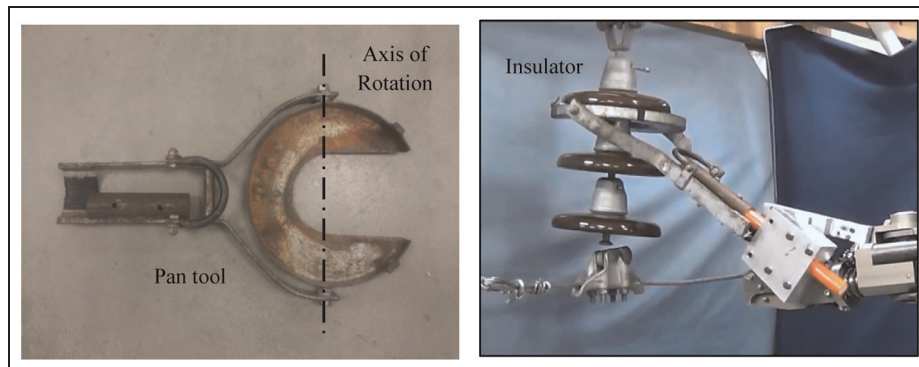
Figure 22. Pan tool being used to remove insulator.
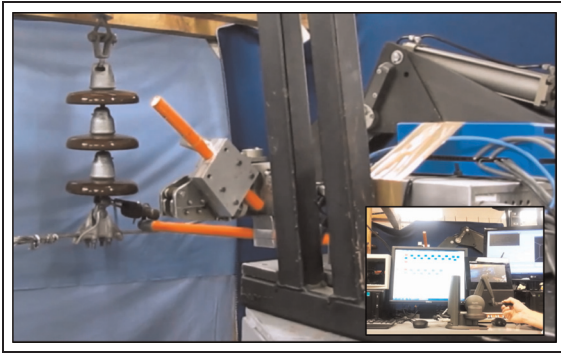
Figure 23. Unpinning the insulator keeper (Task A).
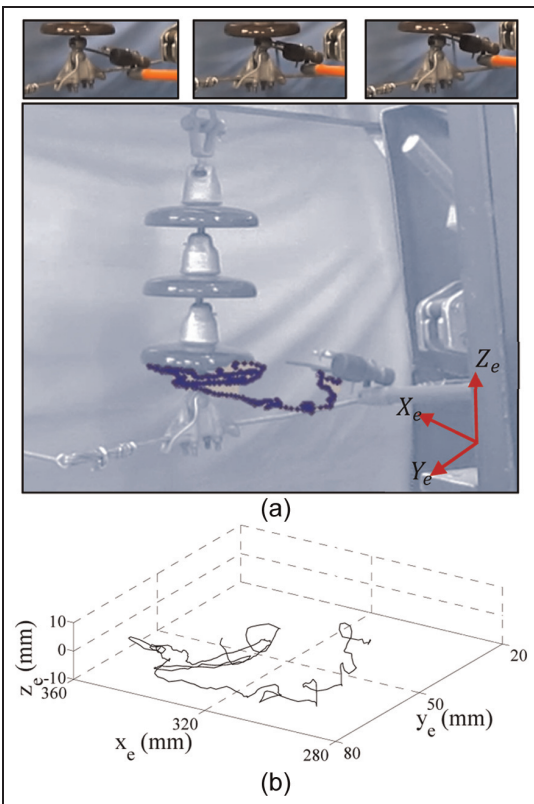
Figure 24. (a) Pulling out the pin using pin puller (Task A), and (b) corresponding work envelope.

Conclusions and future work

This paper documented common challenges in developing a teleoperated robotic setup for live-line maintenance. The features of a novel test facility, designed as a training platform for linemen, were explained. The test station utilized state-of-the-art technologies, control hardware and data acquisition tools. On the control aspect, both unilateral and bilateral controls of hydraulic manipulators were thoroughly examined. With respect to unilateral control, the concept of virtual fixture was employed to reduce master position errors originating from the operator's undesirable hand motion. Extensive
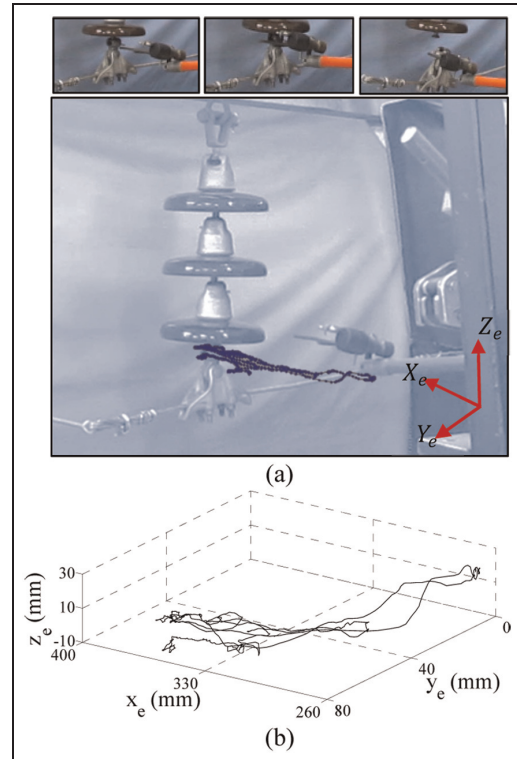
Figure 25. (a) Releasing the lower string using the ball socket adjuster (fork) (Task B), and (b) corresponding work envelope.
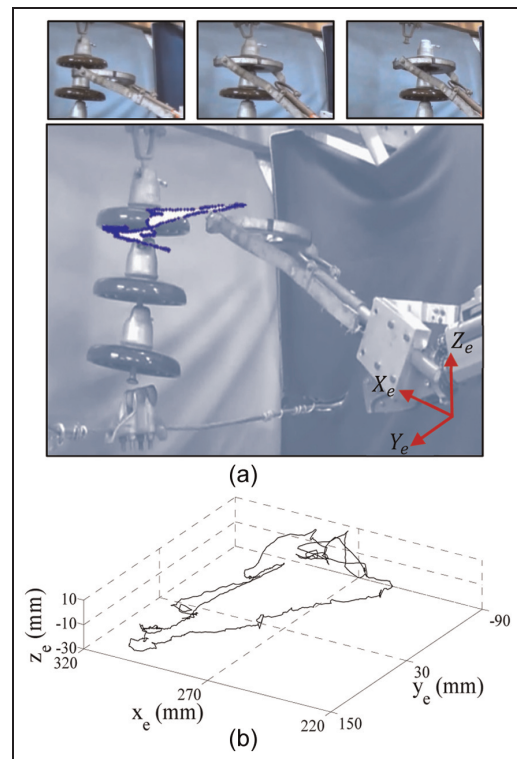
Figure 26. (a) Removing the broken insulator using the pan tool (Task C), and (b) corresponding work envelope.
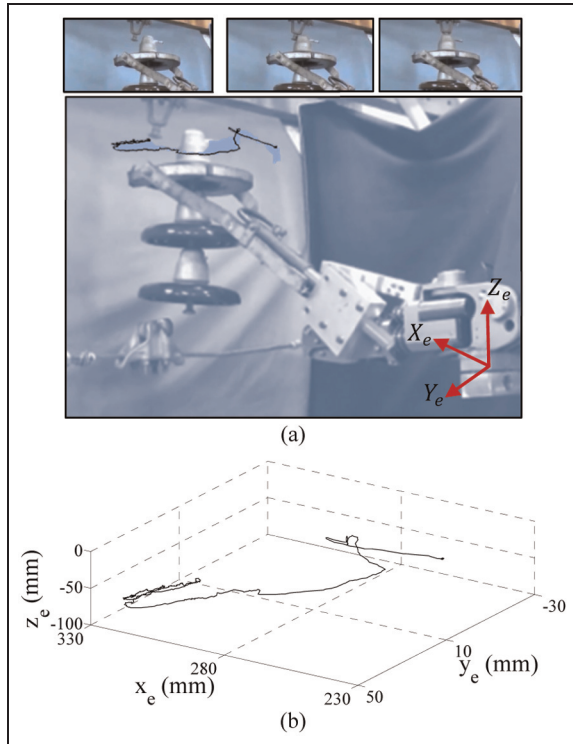
Figure 27. (a) Replacing a new insulator using the pan tool (Task C), and (b) corresponding work envelope.

experimental investigation with experienced linemen has been conducted to demonstrate the effectiveness of the developed test station. However, it was found that virtual fixture could not adequately reduce position errors between the master implement and the slave end-effector. Therefore, the concept of position referenced augmentation force, in bilateral mode, was developed to compensate for positioning errors at the slave end-effector. Combined virtual fixture and augmentation force was shown to decrease position errors at both master implement and slave end-effector. Finally, when the slave manipulator base was excited, the augmentation force scheme performed more effectively than the virtual fixture and the augmented virtual fixture. In addition, various wireless network scenarios were studied, and a lookup table was constructed that allows selecting parameters of a wireless network that guarantee stability and transparency. Laboratory trials by live-line journeymen have been completed to determine adaptability to these robotic procedures compared with current practice.

Future work will focus on deploying the developed robotic setup on to a real field to perform live-line maintenance tasks. Moreover, the available test rig can also be adequately applied in hardware-in-the-loop simulation in other applications such as underwater inspections. The developed test rig with the parallel platform (Stewart platform) allows all possible degrees of freedom such as surge, sway, heave, roll, pitch and yaw as in underwater ROVs. One such application in underwater research area is to test the performance of a manipulator, as part of an ROV for its behavior underwater in six degrees of freedom scenario.
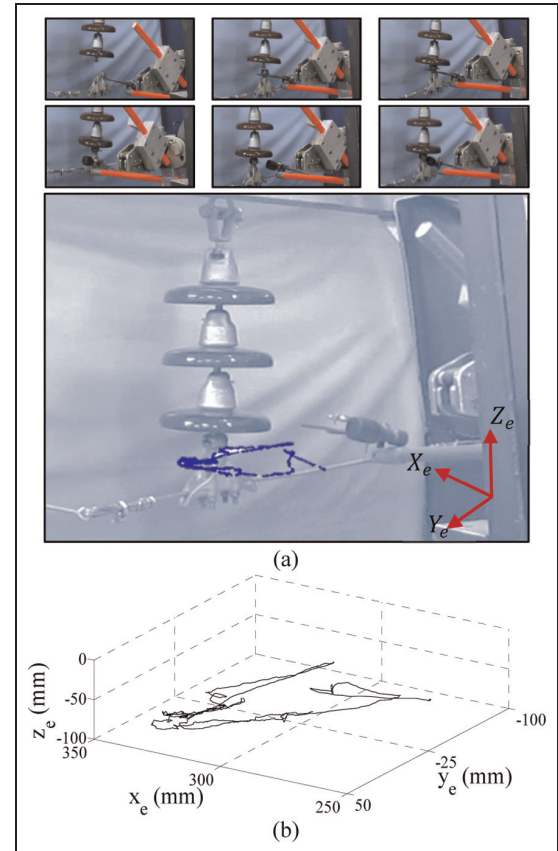
Figure 28. (a) Connecting the lower joint using the ball socket adjuster (fork) (Task B) followed by hammering (Task D), and (b) corresponding work envelope.

Declaration of conflicting interest

The authors declare that there is no conflict of interest.

Funding

References

Abbott JJ, Hager GD and Okamura AM (2003) Steady-hand teleoperation with virtual fixtures. In: *Robot and Human Interactive Communication, 2003. Proceedings. ROMAN 2003*. The 12th IEEE International Workshop. Millbrae, USA, November, pp. 145–151.

Abbott JJ, Marayong P and Okamura AM (2007) Haptic virtual fixtures for robot-assisted manipulation. In: Dr. Sebastian Thrun, Dr. Rodney Brooks and Dr. Hugh Durrant-Whyte (eds) *Robotics Research*. Berlin Heidelberg: Springer, pp. 49–64.

Aracil R, Ferre M, Hernando M, et al. (2002) Telerobotic system for live-power line maintenance: ROBTET. *Control Engineering Practice* 10(11): 1271–1281.

Baheti A, Seshadri S, Kumar A, et al. (2008) Ross: Virtual reality robotic surgical simulator for the da vinci surgical system. In: *2008*

Symposium on Haptic Interfaces for Virtual Environment and Teleoperator Systems, Reno, USA, March 2008, pp. 479–480.

Banthia V, Maddahi Y, Balakrishnan S and Sepehri N (2014) Haptic-enabled teleoperation of base-excited hydraulic manipulators applied to live-line maintenance. In: *2014 IEEE/RSJ International Conference on Intelligent Robots and Systems*, Chicago, USA, September 2014, pp. 1222–1229. IEEE.

Bernhardt R (1987) Macroscopic diversity in frequency reuse radio systems. *IEEE Journal on Selected Areas in Communications* 5(5): 862–870.

Boukhnifer M, Ferreira A and Fontaine JG (2004) Scaled teleoperation controller design for micromanipulation over internet. In: *Robotics and Automation, 2004. Proceedings. ICRA'04. 2004 IEEE International Conference*, New Orleans, USA, April 2004, pp. 4577–4583. IEEE.

Breslau L, Estrin D, Fall K, et al. (2000) Advances in network simulation. *IEEE Computer* 33(5): 59–67.

Cao X, Gu L, Luo G and Wang Y (2015) The adaptive robust tracking control of deep-sea hydraulic manipulator based on backstepping design. In: *OCEANS 2015-MTS/IEEE Washington*, Washington, DC, USA, October 2015, pp. 1–6. IEEE.

Clement G, Vertut J, Fournier R, et al. (1985) An overview of CAT control in nuclear services. In: *Robotics and Automation. Proceedings. 1985 IEEE International Conference*, St. Louis, USA, March 1985, pp. 713–718. IEEE.

Cox DC, Murray RR and Norris AW (1984) 800-MHz attenuation measured in and around suburban houses. *AT&T Bell Laboratories Technical Journal* 63(6): 921–954.

Diolaiti N and Melchiorri C (2002) Teleoperation of a mobile robot through haptic feedback. In: *Haptic Virtual Environments and Their Applications, IEEE International Workshop 2002 HAVE*, Ottawa, Canada, November 2002, pp. 67–72. IEEE.

Eltahir IK (2007) The impact of different radio propagation models for mobile ad hoc networks (MANET) in urban area environment. In: *The 2nd International Conference on Wireless Broadband and Ultra Wideband Communications (AusWireless 2007)*, Sydney, Australia, 27–30 August 2007, pp. 27–30. IEEE.

Funda J and Paul RP (1991) A symbolic teleoperator interface for time-delayed underwater robot manipulation. In: *OCEANS'91. Ocean Technologies and Opportunities in the Pacific for the 90's. Proceedings*, Los Angeles, USA, 1–3 October 1991, pp. 1526–1533. IEEE.

Hokayem PF and Spong MW (2006) Bilateral teleoperation: An historical survey. *Automatica* 42(12): 2035–2057.

Hong SG, Lee JJ and Kim S (1999) Generating artificial force for feedback control of teleoperated mobile robots. In: *Intelligent Robots and Systems, 1999. IROS'99. Proceedings. IEEE/RSJ International Conference*, Kyongju, Korea, 17–21 October 1999, pp. 1721–1726. IEEE.

Jian J, Guoxian Z and Tingyu Z (2009) Design of a mobile robot for the innovation in power line inspection and maintenance. In: *Reconfigurable Mechanisms and Robots, 2009. ReMAR. ASME/IFToMM International Conference*, London, UK, 22–24 June 2009, pp. 444–449. IEEE.

Kang H, Park YS, Ewing TF, et al. (2004) Visually and haptically augmented teleoperation in D&D tasks using virtual fixtures. In: *10th International Conference on Robotics and Remote Systems for Hazardous Environments*, Gainesville, USA, 28–31 March 2004, pp. 466–471.

Kontz ME, Beckwith J and Book WJ (2005) Evaluation of a teleoperated haptic forklift. In: *IEEE/ASME International Conference on Advanced Intelligent Mechatronics*, Monterey, USA, July 2005, pp. 295–300.

Kontz ME and Book WJ (2003) Position/rate haptic control of a hydraulic forklift. In: *ASME 2003 International Mechanical Engineering Congress and Exposition*, Washington, DC, USA, 15–21 November 2003, pp. 801–808.

Lessard J, Robert JM and Rondot P (1995) Evaluaton of working techniques using teleoperation for power line maintenance. In: *Proceedings of Telemanipulator and Telepresence Technologies*, Boston, December 1995, pp. 88–98.

Li M, Ishii M and Taylor RH (2007) Spatial motion constraints using virtual fixtures generated by anatomy. *IEEE Transactions on Robotics* 23(1): 4–19.

Liao S and Fung WK (2011) On network simulation for performance evaluation of real-time Internet-based teleoperation. In: *Robotics and Biomimetics (ROBIO), 2011 IEEE International Conference*, Karon Beach, Thailand, December 2011, pp. 750–755. IEEE.

Lim J, Ko J and Lee J (2003) Internet-based teleoperation of a mobile robot with force-reflection. In: *Control Applications, 2003. CCA 2003. Proceedings of 2003 IEEE Conference*, June 2003, pp. 680–685. IEEE.

Lu S, Ma P, Bingqiang L and BiCui X (2003) Live woking robot for power distribution systems. In: *Control and Automation, 2003. ICCA'03. Proceedings. 4th International Conference*, Montreal, Que., Canada, June 2003, pp. 906–910. IEEE.

Maddahi Y, Zareinia K, Olson T, et al. (2013a) Live-line maintenance training using robotics technology. In: *World Haptics Conference (WHC)*, Daejeon, South Korea, April 2013, pp. 587–592. IEEE.

Maddahi Y, Sepehri N, Liao S, et al. (2013b) Wireless control of a teleoperated hydraulic manipulator with application towards live-line maintenance. In: *ASME/BATH 2013 Symposium on Fluid Power and Motion Control*, Sarasota, Florida, USA, October 2013, pp. V001T01A033–V001T01A033). American Society of Mechanical Engineers.

Maddahi Y, Liao S, Fung WK, et al. (2015a) Selection of network parameters in wireless control of bilateral teleoperated manipulators. *IEEE Transactions on Industrial Informatics* 11(6): 1445–1456.

Maddahi Y, Zareinia K and Sepehri N (2015b) An augmented virtual fixture to improve task performance in robot-assisted live-line maintenance. *Computers & Electrical Engineering* 43: 292–305.

Maddahi Y, Liao S, Fung WK and Sepehri N (2016) Position referenced force augmentation in teleoperated hydraulic manipulators operating under delayed and lossy networks: A pilot study. *Robotics and Autonomous Systems*, 83: 231–242.

Madhani AJ, Niemeyer G and Salisbury JK (1998) The black falcon: A teleoperated surgical instrument for minimally invasive surgery. In: *Intelligent Robots and Systems, Proceedings, 1998 IEEE/RSJ International Conference*, Victoria, Canada, October 1998, pp. 936–944). IEEE.

Matsumoto Y, Katsura S and Ohnishi K (2007) Dexterous manipulation in constrained bilateral teleoperation using controlled supporting point. *IEEE Transactions on Industrial Electronics* 54(2): 1113–1121.

Montambault S and Pouliot N (2003) The HQ LineROVer: Contributing to innovation in transmission line maintenance. In: *Transmission and Distribution Construction, Operation and Live-Line Maintenance, 2003. 2003 IEEE ESMO. 2003 IEEE 10th International Conference*, Orlando, USA, April 2003, pp. 33–40. IEEE.

Moore CA, Peshkin MA and Colgate JE (2003) Cobot implementation of virtual paths and 3D virtual surfaces. *IEEE Transactions on Robotics and Automation* 19(2): 347–351.

Najafi F and Sepehri N (2008) A novel hand-controller for remote ultrasound imaging. *Mechatronics* 18(10): 578–590.

Onat A, Naskali T, Parlakay E and Mutluer O (2011) Control over imperfect networks: Model-based predictive networked control systems. *IEEE Transactions on Industrial Electronics* 58(3): 905–913.

Park JY, Lee JK, Cho BH and Oh KY (2009) Development of inspection robot system for live-line suspension insulator strings in

345kV power transmission lines. In: *2009 13th European Conference on Power Electronics and Applications*, Barcelona, 8–10 September 2009, pp. 1–8.

Rong Z and Rappaport TS (2002) *Wireless Communications: Principles and Practice*, Prentice Hall, New Jersey.

Rösch OJ, Schilling K and Roth H (2002) Haptic interfaces for the remote control of mobile robots. *Control Engineering Practice* 10(11): 1309–1313.

Rosenberg LB (1993) Virtual fixtures: Perceptual tools for telerobotic manipulation. In: *Virtual Reality Annual International Symposium*, Seattle, USA, September 1993, pp. 76–82. IEEE.

Sambo AS, Garba B, Zarma IH and Gaji MM (2012) Electricity generation and the present challenges in the Nigerian power sector. *Journal of Energy and Power Engineering* 6(7): 1050–1059.

Sepehri N, Khayyat AA and Heinrichs B (1997) Development of a nonlinear PI controller for accurate positioning of an industrial hydraulic manipulator. *Mechatronics* 7(8): 683–700.

Song Y, Wang H, Jiang Y and Ling L (2012) AApe-D: A novel power transmission line maintenance robot for broken strand repair. In: *Applied Robotics for the Power Industry (CARPI), 2012 2nd International Conference*, Zurich, Switzerland, September 2012, pp. 108–113. IEEE.

Sun LW, Van Meer F, Bailly Y and Yeung CK (2007) Design and development of a da vinci surgical system simulator. In: *2007 International Conference on Mechatronics and Automation*, August 2007, pp. 1050–1055. IEEE.

Sun W, Zhao Z and Gao H (2013) Saturated adaptive robust control for active suspension systems. *IEEE Transactions on Industrial Electronics* 60(9): 3889–3896.

Suzuki A and Ohnishi K (2013) Frequency-domain damping design for time-delayed bilateral teleoperation system based on modal space analysis. *IEEE Transactions on Industrial Electronics* 60(1): 177–190.

Takaoka K, Yokoyama K, Wakisako H, et al. (2001) Development of the fully-automatic live-line maintenance robot-Phase III. In: *Assembly and Task Planning, 2001, Proceedings of the IEEE International Symposium*, Fukuoka, Japan, 29 May 2001, pp. 423–428. IEEE.

Tavakoli M, Patel RV and Moallem M (2003) A force reflective master-slave system for minimally invasive surgery. In: *Intelligent Robots and Systems, 2003.(IROS 2003). Proceedings. 2003 IEEE/RSJ International Conference*, Las Vegas, USA, October 2003, pp. 3077–3082. IEEE.

Toussaint K, Pouliot N and Montambault S (2009) Transmission line maintenance robots capable of crossing obstacles: State-of-the-art review and challenges ahead. *Journal of Field Robotics* 26(5): 477–499.

Turro N, Khatib O and Coste-Maniere E (2001) Haptically augmented teleoperation. In: *Robotics and Automation, 2001. Proceedings 2001 ICRA. IEEE International Conference*, Seoul, South Korea, 21–26 May 2001, pp. 386–392. IEEE.

Wang B, Chen X, Wang Q, et al. (2010) Power line inspection with a flying robot. In: *Applied Robotics for the Power Industry (CARPI), 2010 1st International Conference*, Montreal, QC, Canada, October 2010, pp. 1–6. IEEE.

Yang Y, Wang Y, Yuan X, et al. (2013) Neural network-based self-learning control for power transmission line deicing robot. *Neural Computing and Applications* 22(5): 969–986.

Yao J, Yang G, Jiao Z and Ma D (2013) Adaptive robust motion control of direct-drive dc motors with continuous friction compensation. In: *Abstract and Applied Analysis* 2013(6): 1–14. Hindawi Publishing Corporation.

Yao J, Jiao Z and Ma D (2014) Extended-state-observer-based output feedback nonlinear robust control of hydraulic systems with backstepping. *IEEE Transactions on Industrial Electronics* 61(11): 6285–6293.

Yu J, Zeng H, Huang L and Wu B (2013) Adaptive output tracking control for a class of high-order nonlinear systems with time-delay. In: *2013 25th Chinese Control and Decision Conference (CCDC)*, Guiyang, China, May 2013, pp. 3838–3843. IEEE.

Zareinia K, Maddahi Y, Sepehri N, et al. (2014) Unilateral control of teleoperated hydraulic manipulators for live-line maintenance: Comparative study. *International Journal of Robotics and Automation* 29(2), 162–174.

Appendix

In Equation (19), T_i and B_i are position vectors of the endpoints of each hydraulic actuator with respect to frames $\{X^t Y^t Z^t\}$ and $\{X^b Y^b Z^b\}$ respectively and are defined as:

$$T_1 = \begin{bmatrix} L_t - r_t \\ -0.5a \\ -H_t \end{bmatrix}; \ T_2 = \begin{bmatrix} L_t - r_t \\ 0.5a \\ -H_t \end{bmatrix};$$

$$T_3 = \begin{bmatrix} 0.5a\sin 60° - (L_t - r_t)\sin 30° \\ (L_t - r_t)\cos 30° + 0.5a\sin 30° \\ -H_t \end{bmatrix}$$

$$T_4 = \begin{bmatrix} -r_t \\ (L_t - r_t)\cos 30° - 0.5a\sin 30° \\ -H_t \end{bmatrix};$$

$$T_5 = \begin{bmatrix} -r_t \\ -(L_t - r_t)\cos 30° + 0.5a\sin 30° \\ H_t \end{bmatrix}$$

$$T_6 = \begin{bmatrix} 0.5a\sin 60 - (L_t - r_t)\sin 30° \\ -(L_t - r_t)\cos 30° - 0.5a\sin 30° \\ -H_t \end{bmatrix}$$

and,

$$B_1 = \begin{bmatrix} r_b \\ -(L_b - r_b)\cos 30° + 0.5c\sin 30° \\ H_b \end{bmatrix};$$

$$B_2 = \begin{bmatrix} r_b \\ (L_b - r_b)\cos 30° - 0.5c\sin 30° \\ H_b \end{bmatrix}$$

$$B_3 = \begin{bmatrix} (L_b - r_b)\sin 30° - 0.5c\sin 60 \\ (L_b - r_b)\cos 30° + 0.5c\sin 30° \\ H_b \end{bmatrix};$$

$$B_4 = \begin{bmatrix} -(L_b - r_b) \\ 0.5c \\ H_b \end{bmatrix}; \ B_5 = \begin{bmatrix} -(L_b - r_b) \\ -0.5c \\ H_b \end{bmatrix}$$

$$B_6 = \begin{bmatrix} (L_b - r_b)\sin 30° - 0.5c\sin 60 \\ -(L_b - r_b)\cos 30° - 0.5c\sin 30° \\ H_b \end{bmatrix}$$

where,

$$L_t = (a + b)\sin 60°, \ L_b = (c + d)\sin 60°$$
$$r_t = \frac{\sqrt{3}}{6}(2a + b), \ r_b = \frac{\sqrt{3}}{6}(2c + d)$$